JACS
JOURNAL OF THE AMERICAN CHEMICAL SOCIETY
Article
pubs.acs.org/JACS

Multilevel Conductance Switching of Memory Device through Photoelectric Effect

Changqing Ye,[†] Qian Peng,[†] Mingzhu Li,*[,†] Jia Luo,[†] Zhengming Tang,[‡] Jian Pei,[‡] Jianming Chen,[†] Zhigang Shuai,[†] Lei Jiang,[†] and Yanlin Song*[,†]

[†]Beijing National Laboratory for Molecular Sciences (BNLMS), Key Laboratory of Organic Solids, Laboratory of New Materials, Institute of Chemistry, Chinese Academy of Sciences, Beijing 100190, China

[‡]College of Chemistry and Molecular Engineering, Peking University, Beijing 100871, P. R. China

Supporting Information

ABSTRACT: A photoelectronic switch of a multilevel memory device has been achieved using a meta-conjugated donor-bridge-acceptor (DBA) molecule. Such a DBA optoelectronic molecule responds to both the optical and electrical stimuli. The device exhibits good electrical bistable switching behaviors under dark, with a large ON/OFF ratio more than 10^6. In cooperation with the UV light, photoelectronic ternary states are addressable in a bistable switching system. On the basis of the CV measurement, charge carriers transport modeling, quantum chemical calculation, and absorption spectra analysis, the mechanism of the DBA memory is suggested to be attributed to the substep charge transfer transition process. The capability of tailoring photoelectrical properties is a very promising strategy to explore the multilevel storage, and it will give a new opportunity for designing multifunctional devices.

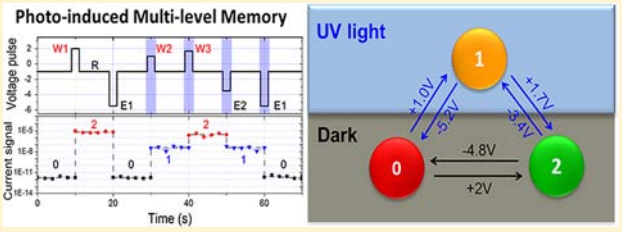

INTRODUCTION

Organic resistive memory devices have attracted increasing attention in recent years,[1−3] attributed to the emerging downscaling limits of the conventional Si-based technologies.[4−6] Organic materials have shown many advantages, including low cost, simple device structure, and flexibility, which are promising for developing next-generation memory devices.[7] In a typical resistive memory, the data storage is based on different conductivities under the applied voltage.[3] Conductivity states, representing different recording data, can be read out nondestructively. No electrical power is required to maintain the conductivity state, which shows the nonvolatile memory effect.[8,9] Currently, most organic resistive memory devices are binary systems consisting of two conductivity states (i.e., ON and OFF states).[10−14] To achieve high-density data storage, the multilevel memory approach is an effective alternative method,[15−19] which can lead to an increasing capacity of 3^n or larger. There have been reports of multilevel organic memory devices based on different mechanisms, such as the redox switch[20−22] or the charge trapping.[18,19] These storage techniques, which use only a single electrical input to operate the switches, are facing the challenge of finding suitable media in the solid state.[19,20] This hindrance has triggered the exploration of storage strategies that can combine multiple physical channels (such as optical, electrical, and magnetic multifunctionality) on a single device.[23−25] Optoelectronic materials can respond to both the optical and electrical stimulus. Utilizing these materials as storage media undergoes diverse electrical switching processes through photoinduced modulation.[26] Such functional optoelectronic materials have already shown practical potential in binary multimode data storage.[27,28]

In this work, we have advanced a novel multilevel memory device using an optoelectronic organic molecule through photoelectronic switching. Utilizing the photoelectric effect can bring evident improvements on the electrical performance of the memory devices.[29,30] Our previous work demonstrated a photoelectric cooperative performance to reduce the power consumption by lowering the threshold voltage of a bilayer memory device.[31] We further found that taking advantage of the photoelectric effect can open up minds for designing new types of appropriate optoelectronic molecules for multilevel storage media.

Here, a meta-conjugated donor-bridge-acceptor (DBA) organic molecule is applied to fabricate the multilevel memory prototype device. This DBA molecule[32] is exploited as the storage medium (Figure 1a) in which triphenylamine (TPA) acts as an electron donor (D) and 2-dicyanomethylen-3-cyano-4,5,5-trimethyl-2,5-dihydrofuran (TCF) acts as an electron acceptor (A).[33] The D−A pair is separated by a meta-conjugated bridge of a 2,7,12-trisubstituted truxene unit. Such a meta-conjugated bridge enhances electronic coupling, promotes charge transfer (CT) from donor to acceptor, and suppresses charge recombination in the reverse direction.[34,35] The DBA compound has an extra photoactive property.[36−38] The photoelectronic effect modifies the bistable switch behaviors of the DBA thin film under modulated UV light. A new light-

Received: January 11, 2012
Published: November 17, 2012

dx.doi.org/10.1021/ja305354y | J. Am. Chem. Soc. 2012, 134, 20053−20059

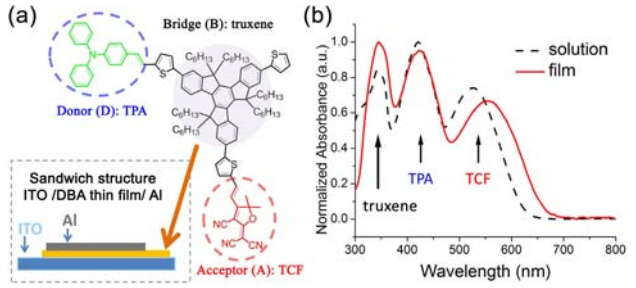

Figure 1. (a) Molecular structure of the donor−bridge−acceptor compound (DBA). Inset: schematic diagram of the ITO/DBA/Al sandwich memory device. (b) Absorption spectra of the DBA molecule in dilute THF solution (10^{-6} mol/L, dash line) and thin film (solid line). The red-shift is related with the formation of molecular aggregation in the film.

induced memory state can be addressable to realize optoelectronic multilevel memory storage. Taking advantage of photoactive molecules under light and asymmetric CT behavior of the meta-conjugated bridge is a very promising strategy to explore the multilevel storage.

EXPERIMENTAL SECTION

Fabrication of the Memory Device. For the fabrication of the memory device, the indium−tin-oxide (ITO) glass substrate was precleaned sequentially with water, ethanol, and acetone, in an ultrasonic bath for 20 min, respectively. The DBA (10 mg/mL) in the mixture of chloroform and toluene (1:1) was spin-coated onto ITO. The thickness of the organic layer was about 100 nm. Aluminum top electrodes of 0.2 × 0.8 mm^2 in area and *ca.* 0.3 μm in thickness were thermally evaporated onto the organic molecular surface at about 10^{-7} Torr through a shadow mask. The macroscopic $I-V$ characteristics of the devices were characterized under ambient conditions, using a Keilthley 4200-SCS semiconductor system. The voltages were changed in steps of 0.05 V.

A UV LED lamp with the wavelength of 405 nm was used as the UV illumination source. The absorption spectrum of the film was measured with a fiber optic UV−vis−IR spectrometer (Ocean Optic HR 4000 CG).

Quantum Chemical Calculation. The density functional theory (DFT) and time-dependent DFT (TDDFT) calculations were performed using the hybrid functional B3LYP[39−41] with the basis set 6-31G* for three compounds, such as **D−B−A** in the neutral, anion, and cation states; **D−B** (TPA-truxene unit) in the neutral and cation states, and **B−A** (TCF-truxene unit) in the neutral and anion states (for molecule structures, see Figure S1). Here, the alkyl groups on the core were not included, since they did not much affect the equilibrium geometry and the electronic properties.[42] First, the electronic ground states were optimized for all the above compounds via DFT. Then, the excitation energies and the corresponding oscillator strengths of the low-lying states were calculated with TD-DFT and summarized in Table 1. All calculations were performed with Gaussian 09 (revision A.02).[43] Orbital pictures were prepared with GaussView visual software.

RESULTS AND DISCUSSION

Typical UV−vis spectra of DBA both in solution and in thin film were compared in Figure 1b. The dashed line shows the absorbance features of DBA in dilute tetrahydrofuran (THF) solution (10^{-6} mol/L). The absorbance of the spin-coated DBA thin film (sold line) exhibited an absorption peak at 554 nm, which was a 30 nm red-shift relative to that peak in solution (524 nm). Compared to that in solution, the onset of the absorbance in thin film also moved from 680 to 720 nm. Such a red-shift was related with the formation of molecular aggregation in the thin film.[13] The current−voltage ($I-V$) characteristics of the Al/DBA/ITO sandwich memory device were measured (as shown in Figure 2a). The initial four sweeps

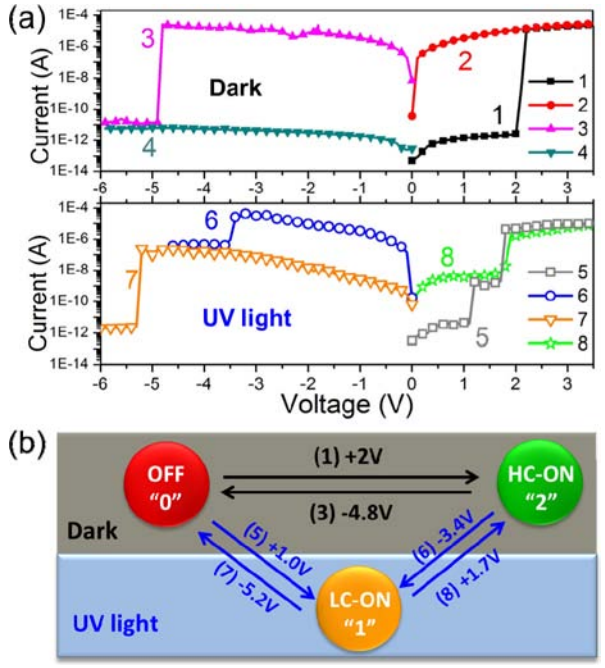

Figure 2. (a) $I-V$ characteristics of the memory device. Sweeps 1−4 were scanned under the dark. Sweeps 5−8 were scanned under the UV light of 1.01 mW/cm^2. (b) Schematic graph showing the possible transitions and threshold voltage among three states: "0" (OFF state); "1" (low-conductivity state, LC-ON); "2" (high-conductivity state, HC-ON). In cooperation with the UV light, a new LC-ON state was addressable. A photoinduced multilevel memory device has been achieved. The arrows among three states showed the switching thresholds and the corresponding $I-V$ sweeps in part a.

Table 1. Summary of Calculated Absorption Peaks with Oscillator Strengths (f) Shown in the Brackets

	calcd abs peak		
compd	TPA-truxene	TCF-truxene	truxene
D−B−A	470.13 nm (f = 1.6897)	527.58 nm (f = 1.5707)	
D−B	461.90 nm (f = 2.1759)		
B−A		509.43 nm (f = 1.3209)	344.71 nm (f = 1.5707)
$(\mathbf{D-B-A})^+$	648.52 nm (f = 0.8349)		
$(\mathbf{D-B-A})^-$	675.85 nm (f = 0.8353)		
$(\mathbf{D-B})^+$	653.01 nm (f = 0.9597)		
$(\mathbf{B-A})^-$		674.09 nm (f = 0.8760)	

dx.doi.org/10.1021/ja305354y | J. Am. Chem. Soc. 2012, 134, 20053−20059

were scanned in the dark environment. In the first sweep from 0 V to +3.5 V, an abrupt increase in current was observed at the switching threshold voltage of +2.0 V, indicating the transition from the OFF state to a high-conductivity state (HC-ON). The device remained at this HC-ON state in the next sweep from 0 V to +3.5 V (sweep 2). The device returned to the OFF state in the reverse sweep as the voltage approached −4.8 V (sweep 3). The device showed a low-conductivity state again in the followed sweeping from 0 V to −6 V (sweep 4).

To realize photoinduced multilevel memory storage, the device was tested under UV light (405 nm) of 1.01 mW/cm^2. In sweep 5 from 0 to +3.5 V, two abrupt increases of current were observed at switching threshold voltages of +1.0 V and +1.7 V. The transition from the OFF state to a new intermediate low-conductivity state (LC-ON) occurred at +1.0 V. The LC-ON state was sustained until +1.7 V and then turned to the HC-ON state. The photoelectric effect reduced the switching threshold voltage of the HC-ON state to +1.7 V under UV light, which was lower than the threshold in the dark (+2.0 V). In subsequent reverse sweep 6 with UV light, the current decreased from 2.53 × 10^{-5} A to 4.07 × 10^{-7} A at −3.4 V. The device under UV light turned from the HC-ON state to the LC-ON state. This was different from the case for sweep 3, in which the device was directly switched from the HC-ON state to the OFF state. This LC-ON state was retained until −5.2 V and then turned to the OFF state (sweep 7). The LC-ON state can also switch to the HC-ON state again during another positive forward sweep at +1.7 V under UV light (sweep 8).

In order to encode the measured current signals into information data for a memory device, we designated "0" as the OFF state, "1" as the intermediate LC-ON state, and "2" as the HC-ON state, respectively. Figure 2b summarizes the transitions of the device and the switching thresholds among three-level storage signals. In the dark scanning environment, the device only showed a typical electrical bistable switching behavior between "0" and "2" during the sweep 1−4. In cooperation with the UV light, a new "1" state was addressable. The "1" state was "written" through the "0" by the appropriate UV light and a positive voltage of +1.0 V, or through the "2" by the UV light and a negative voltage of −3.4 V. The "1" was "erased" to "0" by a negative voltage pulse larger than −5.2 V, or "rewritten" to "2" by a positive voltage pulse large than +1.7 V under UV light. Here, the UV light was applied for assisting the LC-ON conductive switching. The LC-ON conductance state can be maintained stable after the transition without light irradiation. Therefore, a photoinduced ternary memory device has been achieved. Besides, this multilevel memory device has potential in encrypted storage, for the "1" can only be switched to under a cooperative action of UV light irradiation and proper voltage.

To demonstrate that the Al/DBA/ITO sandwich device can serve as a prototype multilevel memory, write-read-erase switching cycles were performed (Figure 3). A voltage of +2.0 V (W1) was applied to write a datum of "2" to the device. This voltage switched the device from the initial "0" state to the "2" state. The states were read by a low voltage (R: −1.0 V in our experiment). The current at the "2" state under the read voltage was of the order of 10^{-5} A. This "2" state was erased by a voltage of −5.5 V (E1), which returned the device to the "0" state (the current order of 10^{-12} A). Under the UV light (1.01 mW/cm^2), the LC-ON state was addressable. A combination of the UV light and a voltage pulse of +1.0 V (W2) was applied to

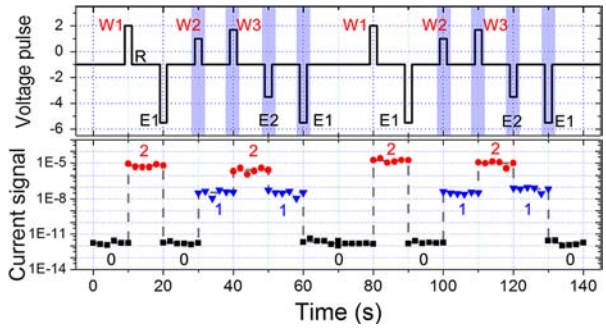

Figure 3. Multilevel write−read−erase cycles of the DBA prototype device. The blue zone covered on the voltage curve demonstrated the UV light was applied at the same time. W1, W2, W3, R, E1, and E2 in the upper curve mean different operating voltage pulses for write, read, and erase, respectively.

write the "1" state from initial the "0" state. The current was of the order of 10^{-8} A. This "1" state was further rewritten to the "2" state by a larger voltage of +1.7 V (W3). Conversely, the "2" state was switched to the "1" state by a negative voltage of −3.5 V (E2) under the UV light. This "1" state can also be erased to the "0" state by the voltage of −5.5 V (E1). These write−read−erase switching cycles have shown good repeatability for multilevel memory storage.

The stability of the ITO/DBA/Al sandwich memory device under a constant stress of −1.0 V was evaluated under ambient conditions (Figure 4a). No current decay for each state ("0, 1,

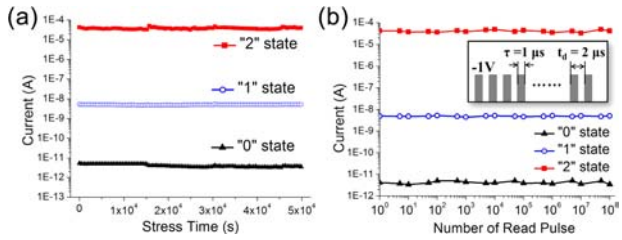

Figure 4. (a) Stability of the Al/DBA/ITO device at the "0, 1, 2" states under a constant stress (−1 V) for 10 h. (b) Effect of read pulse cycles on the device at the "0, 1, 2" states. The inset shows the pulses used for this measurement. The continuous read pulse has a peak voltage of −1 V. The pulse width (τ) is 1 μs, and a pulse period (t_d) is 2 μs.

2" states) was observed in 10 h during the test. The effect of read pulses on the device at different states ("0, 1, 2") was also investigated (Figure 4b). The inset in Figure 4b shows the pulses used for the measurements. The pulse has a peak voltage of −1 V. The pulse width (τ) is 1 μs, and the pulse period (t_d) is 2 μs. No current decay was observed after more than one hundred million (10^8) read cycles. Neither the voltage stress nor the read pulses caused the state transition. Thus, the memory device is insensitive to different readout methods (constant voltage stress or reading pulses). The I−V curves at each state show little change in 7 months even without the protection of encapsulation, which is a benefit of memory devices (see Supporting Information, Figure S3). All these results reveal that the prototype memory device based on DBA molecules has a potential application for multilevel memory storage and encrypted storage.

The conductance switching of resistive memories can be ascribed to the different transport behaviors (trapping or transporting) of charge carriers among organic molecules under

dx.doi.org/10.1021/ja305354y | J. Am. Chem. Soc. 2012, 134, 20053−20059

an electric field.[2] The measured $I-V$ curves at different states of the DBA device were fitted with appropriate charge transport models. For the $I-V$ curve at the "0" state, the plot of $\ln(I)$ versus $V^{1/2}$ was well fitted to a line in the voltage range from 0 to 2 V before the electrical transition (Figure 5a). Such a linear

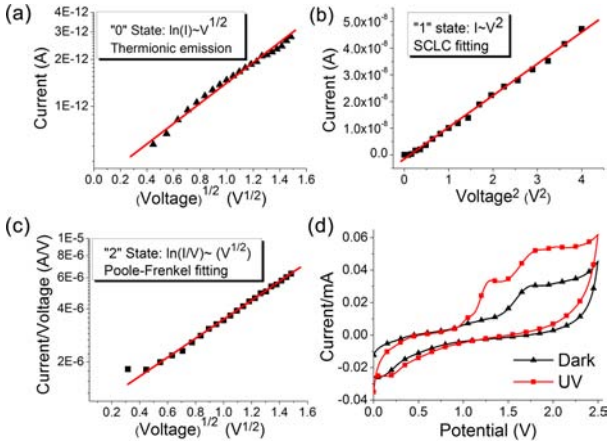

Figure 5. Analysis of $I-V$ characteristics for the device: (a) thermionic emission at the "0" state; (b) space-charge-limited current (SCLC) model at the "1" state; (c) Poole–Frenkel emission model at the "2" state; (d) cyclic voltammograms of the DBA thin film under dark vs UV light conditions.

relation suggests that the conduction mechanism at the "0" state can be considered as the thermionic emission process.[44] The conduction is dominated by charge injection.[8] The $I-V$ curve at the "1" state was fitted to a linear relationship between I and V^2, in the voltage range from 0 to 1.7 V (Figure 5b). The space-charge-limited current (SCLC) model[39] can be satisfactorily fitted to the $I-V$ characteristics at the "1" state. When the memory device was switched to the "2" state, a linear relation was observed between $\ln(I/V)$ and $V^{1/2}$ (Figure 5c). The $I-V$ curve can be fitted by the Poole–Frenkel (PF) emission model.[45,46] The PF conduction mechanism is dominated by charge transport though the bulk materials filled with electrically charged defects.[8] Therefore, the DBA memory device showed different transport behaviors at different conductivity states: the injection-dominated mechanism at the "0" state, the trap-limited mechanism at the "1" state, and the charge-transport-dominated mechanism at the "2" state. The conductivity switching was induced by the CT occurring in the DBA thin film. Different transport behaviors can be ascribed to disparate CT complexes existing at different states.

Cyclic voltammetry (CV) can readily provide qualitative information about the oxidation states and the electron transfer reactions of a redox system. The CV responses of the DBA thin film under dark and UV conditions were compared in Figure 5d. The film was made by drop-casting the $CHCl_3$ solution of the DBA compound on a glassy carbon electrode. The electrolyte was 0.1 mol/L n-Bu_4NPF_6 in acetonitrile. Ag/AgCl was chosen as the reference electrode. The scan rate was set at 100 mV s^{-1}. The CV of the DBA thin film scanned under dark showed an oxidation wave at +1.7 V. When the CV was scanned under the UV light, the CV exhibited two oxidation peaks appearing at +1.29 V and +1.77 V. It demonstrated that there was a stepwise oxidation process that occurred when the DBA thin film was under the light. This result supported the idea that the conductivity of photoinduced ternary DBA memory device can first switch to the LC-ON ("1") state and then to the HC-ON ("2") state under UV light by a photoelectric effect.

UV–vis absorbance spectra can directly confirm the formation of different CT complexes.[47−50] The absorption spectra of the DBA thin film at different states showed distinct features in Figure 6a. In Figure 6b, the experimental spectrum

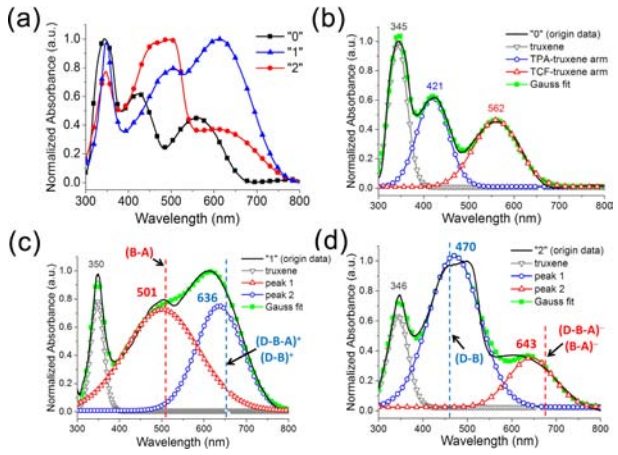

Figure 6. (a) Absorption spectra of the DBA thin film at the "0" state (black line, ■); at the "1" state (blue line, ▲); and at the "2" state (red line, ●). The UV–vis spectra proved that different CT complexes were formed during the switching. The experimental spectra of (b) the "0" state; (c) the "1" state; and (d) the "2" state (black solid line) can be separated into three distinct components by the Gaussian peak fit method. They can be identified as different electronic structures. Calculated absorption peaks of possible components were shown by the dash line in parts c and d.

of the DBA thin film at the "0" state can be separated into three distinct components by the Gaussian peak fit method: peaks at 345, 421, and 562 nm, respectively. Compared with the dominating peaks at the "0" state, both the two low-energy peaks (i.e., absorption band at long wavelength) have remarkable red shifts at the "1" and "2" states, while the high-energy peak (absorption at *ca.* 345 nm) is barely changed. Moreover, the two low-energy peaks exhibited much different characters between the "1" state and the "2" state. These indicate that different excitation processes occurred and different CT complexes were formed in the DBA thin film during the switching process.

In order to identify the electronic structures of different absorbance peaks and understand the relationship between structure and property, quantum chemical calculations were performed. First, the electronic ground states for **D–B–A** compound and two other model compounds (**D–B** and **B–A**) at neutral and charged states were optimized. Then, the calculated absorption peaks and the corresponding oscillator strengths, which are the dimensionless quantities to measure the intensity of absorption, were calculated using TDDFT and summarized in Table 1. Furthermore, the detailed information of transition properties and main configurations was given in Table S1 (See Supporting Information).

From Table 1 and Table S1 the following can be concluded: for **D–B–A** compound, the absorption peak at 470.13 nm mainly stemmed from the transition from HOMO (localized at the TPA arm) to LUMO+1 (localized at TPA-truxene), which is the same as the transition in model compound **D–B** at 461.90 nm, while the absorption peak at 527.58 nm mainly

dx.doi.org/10.1021/ja305354y | J. Am. Chem. Soc. 2012, 134, 20053–20059

came from the transition from HOMO-3 (TCF-truxene) to LUMO (TCF arm), which is the same as the transition in model compound **B**−**A** at 509.43 nm. Additionally, the transition of the high-energy peak of **B**−**A** at 344.71 nm mainly happened on the truxene core. This information shows that the three peaks of DBA in the experimental spectrum in the "0" state are assigned to the excitation of truxene, TPA-truxene, and TCF-truxene, respectively (seen in Figure 6b), although there is a little difference between the calculated absolute values in the gas and the counterparts in the thin film due to the molecular aggregation. The absorptions of the TPA and TCF arms are independent from each other when two arms are joined together in D−B−A. That is to say, donor and acceptor units are intercepted at the central meta-conjugated truxene core, which acts as a mediator for the CT process from **D** to **A**. The positive and negative charges can be segregated by the meta-conjugated bridge and localized in the donor or acceptor. Furthermore, this meta-conjugated bridge can also increase the back CT energy barrier and possibly prevent the recombination of segregated charges.[30,34]

The calculated absorption peaks of $(\mathbf{D}\text{-}\mathbf{B}\text{-}\mathbf{A})^+$ and $(\mathbf{D}\text{-}\mathbf{B}\text{-}\mathbf{A})^-$ showed remarkable red shifts compared to that of the neutral **D-B-A**. The excitation in $(\mathbf{D}\text{-}\mathbf{B}\text{-}\mathbf{A})^+$ (648.52 nm) is very similar to that in $(\mathbf{D}\text{-}\mathbf{B})^+$ (653.01 nm). While the excitation of $(\mathbf{D}\text{-}\mathbf{B}\text{-}\mathbf{A})^-$ at 675.85 nm is ascribed to the charge transfer from the TCF-arm to the TPA-arm, extremely different from that happened on $(\mathbf{B}\text{-}\mathbf{A})^-$ (674.09 nm). Transition details were shown in Table S1 (see Supporting Information). Therefore, the following can be inferred: (1) At the "1" state, the absorption peak at 501 nm is identified as the excitation of neutral TCF-truxene arm, while the excitation of the neutral TPA-truxene arm is missing. A reasonable prediction can be drawn that another peak at 636 nm is ascribed to the excitation of the cation state of the TPA-truxene arm (seen in Figure 6c). (2) At the "2" state, the excitation of the neutral TPA-truxene arm appears again at 470 nm. So the mixing of the excitation of the anion state of the TCF-truxene arm contributes to another peak at 636 nm (seen in Figure 6d).

On the basis of the above CV measurement, charge carriers' transport modeling, absorption spectra analysis, and quantum chemical calculations, we suggested that the electronic transitions of the switching could be attributed to the substep charge transfer processes through the cooperation of UV light and electrical field to achieve a multilevel conductance switching.

Possible carriers' migration processes between DBA molecules and electrodes at each state and plausible electronic switching processes are proposed in Figure 7. Electrostatic potentials (ESP) of the D−B−A at neutral and charged states verified the electronic processes at different conductance states. The potential surfaces of the D−B−A molecule at the neutral state had some negative ESP regions (red in Figure 7a), which arise from the electron-acceptor group (the TCF segment). These negative regions can serve as "traps" to block the mobility of charge carriers (Figure 7a; Figure S5a).[10] Besides, at the "0" state, the energy barrier between the Al electrode and the DBA layer is as large as 0.95 eV, which also blocks the electron migration (Figure 7a; Figure S4d). So it is easy to understand the low conductance of the DBA thin film at the "0" state.

Applying an UV light of 405 nm, electrons at the HOMO can be excited to the LUMO+1 within the TPA unit (see Supporting Information, Figure S4a,c; Table S1: D−B−A, Transition S0 → S5). External light could provide activation energy and promote the photoinduced electron transfer. The activated TPA groups (D*) near the anode could be easily oxidized under proper forward voltage. As a result, more holes are transported from the interface near the anode to the bulk (hole injection), leading to an accumulation of space charges and a redistribution of the electric field. The current of the thin film turns to obey the SCLC model. The ESP surface of $(\mathbf{D}\text{−}\mathbf{B}\text{−}\mathbf{A})^+$ shows that the negative regions (in red) decrease and that the traps are partly filled (Figure 7b; Figure S5b),

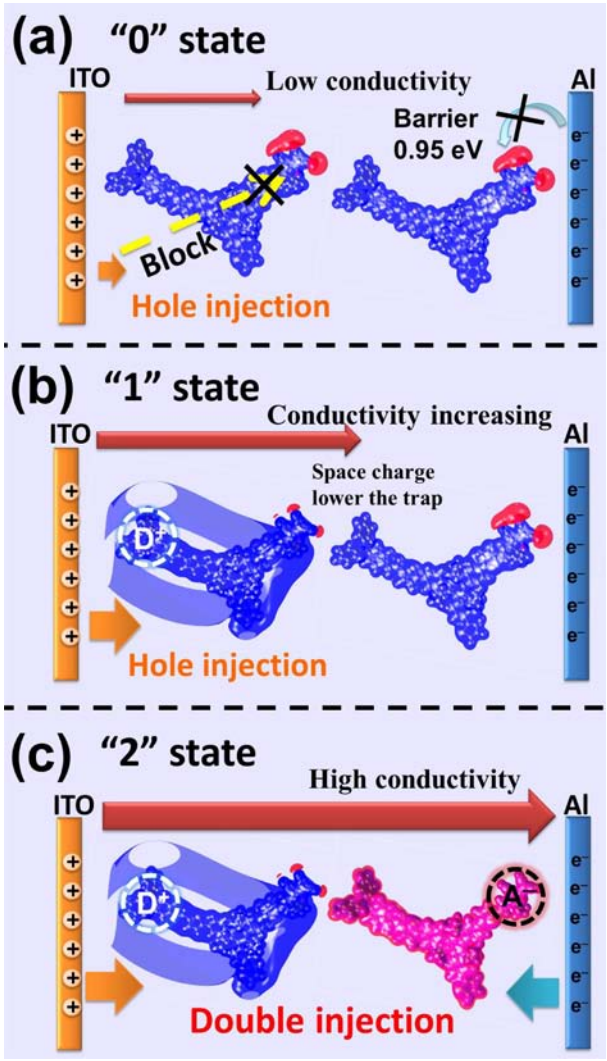

Figure 7. Possible carriers' migration processes between DBA molecules and electrodes at each state are proposed. The electron densities of the molecule are presented through the molecular electrostatic potential (ESP) surface. (a) The neutral D−B−A molecule at the "0" state (density isoval = 0.04). Some negative ESP regions (in red) can serve as traps and block the carriers. (b) At the "1" state, the DBA molecule near the anode can be easily oxidized through the photoelectric effect. Negative ESP regions decrease, and the traps are partly filled at the cation state of DBA (density isoval = 0.04/outer and 0.1/inner). The hole injection is easier, and the thin film has better conductivity. (c) The electrons can exceed the Schottky barrier near the cathode. $(D^+\text{−}B\text{−}A^-)$ or a pair of $(D^+\text{−}B\text{−}A)$ and $(D\text{−}B\text{−}A^-)$ are probably to be formed. The molecular surface of the $(D\text{−}B\text{−}A)^-$ had a continuous ESP (density isoval = 0.01) along the conjugated backbone, which indicated that charge carriers can migrate much more easily through this open channel.

dx.doi.org/10.1021/ja305354y | J. Am. Chem. Soc. 2012, 134, 20053−20059

compared with the neutral state of the **D**−**B**−**A** molecule. The hole injection is easier and the thin film has better conductivity at the "1" state. The radical cation of the TPA unit could be delocalized from the central nitrogen atom to the ring carbons, which could stabilize the charge on the TPA (Figure. S6). Here, these DBA molecules may undergo a distinctive electrical process on the donor segment ($\mathbf{D} \rightarrow \mathbf{D}^* \rightarrow \mathbf{D}^+$) through a photoelectric effect. This differs from the normal redox process, in which the holes must be transported to the acceptor sites by an applied voltage before charge trapping.[51] Thus, a light-induced memory state is addressable to complement the multilevel memory storage.

As the electrical field keeps increasing the switching threshold voltage of the "2" state, the electrons could exceed the Schottky barrier near the cathode (Figure S4d), which leads to double injection. CT complexes such as ($\mathbf{D}^+$−**B**−$\mathbf{A}^-$) or a pair of ($\mathbf{D}^+$−**B**−**A**) and (**D**−**B**−$\mathbf{A}^-$), are probably to be formed in the film. The molecular surface of the ($\mathbf{D}$−**B**−$\mathbf{A}$)$^-$ has a continuous ESP along the conjugated backbone, and the traps are filled (Figure 7c and Figure S5c). The meta-conjugated truxene core can block the recombination of segregated charges. Thus, a stable environment was created in which charge carriers can migrate easily through this open channel.

CONCLUSION

In conclusion, a DBA meta-conjugated molecule has been applied for developing the photoinduced multilevel memory device. The DBA compound shows good electrical bistable switching behaviors between "0" (OFF) and "2" (HC-ON) states under dark, with a large ON/OFF ratio more than 10^6. In cooperation with the UV light, a new "1" (LC-ON) state is addressable. This "1" state is "written" from the "0" state, by a combination of the UV light and a positive voltage of +1.0 V, or from the "2" (HC-ON) state, by a combination of the UV light and a negative voltage of −3.4 V. Based on the CV measurement, charge carriers transport modeling, quantum chemical calculation, and absorption spectra analysis, the mechanism of the DBA photoinduced multilevel memory is attributed to the substep charge transfer processes through the cooperation of UV light and electrical field. The write-read-erase switching cycles among the ternary conductivity ("0, 1, 2") states reveal that the capability of tailoring photoelectrical properties provides a new approach to multilevel memory and encrypted storage. The photoelectric effect will open up new opportunities for designing multifunctional devices.

ASSOCIATED CONTENT

Supporting Information

Computational details and molecular orbitals. This material is available free of charge via the Internet at http://pubs.acs.org.

AUTHOR INFORMATION

Corresponding Author

ylsong@iccas.ac.cn; mingzhu@iccas.ac.cn

Notes

The authors declare no competing financial interest.

ACKNOWLEDGMENTS

The authors thank Professor Yongfang Li and Dr. Chao Liu from Institute of Chemistry for their helpful discussions; Professor Dongxia Shi and Dr. Congli He from Institute of Physics for their help in the stability and reliability measurements; and Professor Shixuan Du and Dr. Jinbo Pan from Institute of Physics for their helpful molecular modeling. This work is supported by the National Nature Science Foundation (Grant Nos. 51173190, 21003132, 21073203, 91127038, and 21121001) and the 973 Program (2009CB930404, 2011CB932303, 2011CB808400, and 2013CB933004).

REFERENCES

(1) Jiang, G. Y.; Song, Y. L.; Guo, X. F.; Zhang, D. Q.; Zhu, D. B. *Adv. Mater.* **2008**, *20*, 2888.
(2) Ling, Q. D.; Liaw, D. J.; Zhu, C. X.; Chan, D. S. H.; Kang, E. T.; Neoh, K. G. *Prog. Polym. Sci.* **2008**, *33*, 917.
(3) Scott, J. C.; Bozano, L. D. *Adv. Mater.* **2007**, *19*, 1452.
(4) Chau, R.; Doyle, B.; Datta, S.; Kavalieros, J.; Zhang, K. *Nat. Mater.* **2007**, *6*, 810.
(5) Lu, W.; Lieber, C. M. *Nat. Mater.* **2007**, *6*, 841.
(6) Raymo, F. M. *Adv. Mater.* **2002**, *14*, 401.
(7) Cho, B.; Song, S.; Ji, Y.; Kim, T. W.; Lee, T. *Adv. Funct. Mater.* **2011**, *21*, 2806.
(8) Chu, C. W.; Ouyang, J.; Tseng, H. H.; Yang, Y. *Adv. Mater.* **2005**, *17*, 1440.
(9) Ling, Q. D.; Lim, S. L.; Song, Y.; Zhu, C. X.; Chan, D. S. H.; Kang, E. T.; Neoh, K. G. *Langmuir* **2007**, *23*, 312.
(10) Ling, Q. D.; Song, Y.; Lim, S. L.; Teo, E. Y. H.; Tan, Y. P.; Zhu, C. X.; Chan, D. S. H.; Kwong, D. L.; Kang, E. T.; Neoh, K. G. *Angew. Chem., Int. Ed.* **2006**, *45*, 2947.
(11) Ouyang, J. Y.; Chu, C. W.; Szmanda, C. R.; Ma, L. P.; Yang, Y. *Nat. Mater.* **2004**, *3*, 918.
(12) Hu, J.; Li, Y.; Ji, Z.; Jiang, G.; Yang, L.; Hu, W.; Gao, H.; Jiang, L.; Wen, Y.; Song, Y.; Zhu, D. *J. Mater. Chem.* **2007**, *17*, 3530.
(13) Shang, Y. L.; Wen, Y. Q.; Li, S. L.; Du, S. X.; He, X. B.; Cai, L.; Li, Y. F.; Yang, L. M.; Gao, H. J.; Song, Y. *J. Am. Chem. Soc.* **2007**, *129*, 11674.
(14) Ling, Q. D.; Chang, F. C.; Song, Y.; Zhu, C. X.; Liaw, D. J.; Chan, D. S. H.; Kang, E. T.; Neoh, K. G. *J. Am. Chem. Soc.* **2006**, *128*, 8732.
(15) Rozenberg, M. J.; Inoue, I. H.; Sanchez, M. J. *Phys. Rev. Lett.* **2004**, *92*, 178302.
(16) Wang, J.; Stucky, G. D. *Adv. Funct. Mater.* **2004**, *14*, 409.
(17) Jung, Y.; Lee, S. H.; Jennings, A. T.; Agarwal, R. *Nano Lett.* **2008**, *8*, 2056.
(18) Lee, J. S.; Kim, Y. M.; Kwon, J. H.; Sim, J. S.; Shin, H.; Sohn, B. H.; Jia, Q. X. *Adv. Mater.* **2011**, *23*, 2064.
(19) Li, H.; Xu, Q. F.; Li, N. J.; Sun, R.; Ge, J. F.; Lu, J. M.; Gu, H. W.; Yan, F. *J. Am. Chem. Soc.* **2010**, *132*, 5542.
(20) Simao, C.; Mas-Torrent, M.; Casado-Montenegro, J.; Oton, F.; Veciana, J.; Rovira, C. *J. Am. Chem. Soc.* **2011**, *133*, 13256.
(21) Lee, T.; Kim, S. U.; Min, J.; Choi, J. W. *Adv. Mater.* **2010**, *22*, 510.
(22) Li, C.; Fan, W. D.; Lei, B.; Zhang, D. H.; Han, S.; Tang, T.; Liu, X. L.; Liu, Z. Q.; Asano, S.; Meyyappan, M.; Han, J.; Zhou, C. W. *Appl. Phys. Lett.* **2004**, *84*, 1949.
(23) Liu, Z. F.; Hashimoto, K.; Fujishima, A. *Nature* **1990**, *347*, 658.
(24) Browne, W. R.; Pollard, M. M.; de Lange, B.; Meetsma, A.; Feringa, B. L. *J. Am. Chem. Soc.* **2006**, *128*, 12412.
(25) Itkis, M. E.; Chi, X.; Cordes, A. W.; Haddon, R. C. *Science* **2002**, *296*, 1443.
(26) Kronemeijer, A. J.; Akkerman, H. B.; Kudernac, T.; van Wees, B. J.; Feringa, B. L.; Blom, P. W. M.; de Boer, B. *Adv. Mater.* **2008**, *20*, 1467.
(27) Jiang, G. Y.; Song, Y. L.; Wen, Y. Q.; Yuan, W. F.; Wu, H. M.; Yang, Z.; Xia, A. D.; Feng, M.; Du, S. X.; Gao, H. J.; Jiang, L.; Zhu, D. B. *ChemPhysChem* **2005**, *6*, 1478.
(28) Li, H.; Wen, Y. Q.; Li, P. W.; Wang, R. M.; Li, G.; Ma, Y.; Yang, L. M.; Song, Y. L.; Yang, Q. L.; Zhu, D. B. *Appl. Phys. Lett.* **2009**, *94*, 163309.
(29) Noh, Y. Y.; Ghim, J.; Kang, S. J.; Baeg, K. J.; Kim, D. Y.; Yase, K. *J. Appl. Phys.* **2006**, *100*, 094501.

(30) Iimori, T.; Naito, T.; Ohta, N. *J. Phys. Chem. C* **2009**, *113*, 4654.
(31) Ma, Y.; Wen, Y. Q.; Wang, J. X.; Shang, Y. L.; Du, S. X.; Pan, L. D.; Li, G.; Yang, L. M.; Gao, H. J.; Song, Y. L. *J. Phys. Chem. C* **2009**, *113*, 8548.
(32) Tang, Z. M.; Lei, T.; Wang, J. L.; Ma, Y. G.; Pei, J. *J. Org. Chem.* **2010**, *75*, 3644.
(33) Yang, J. S.; Huang, H. H.; Ho, J. H. *J. Phys. Chem. B* **2008**, *112*, 8871.
(34) Thompson, A. L.; Ahn, T. S.; Thomas, K. R. J.; Thayumanavan, S.; Martinez, T. J.; Bardeen, C. J. *J. Am. Chem. Soc.* **2005**, *127*, 16348.
(35) Gaab, K. M.; Thompson, A. L.; Xu, J. J.; Martinez, T. J.; Bardeen, C. J. *J. Am. Chem. Soc.* **2003**, *125*, 9288.
(36) Gust, D.; Moore, T. A.; Moore, A. L. *Acc. Chem. Res.* **2001**, *34*, 40.
(37) Wasielewski, M. R. *Chem. Rev.* **1992**, *92*, 435.
(38) Duan, C. H.; Chen, K. S.; Huang, F.; Yip, H. L.; Liu, S. J.; Zhang, J.; Jen, A. K. Y.; Cao, Y. *Chem. Mater.* **2010**, *22*, 6444.
(39) Murgatro, Pn *J. Phys. D: Appl. Phys.* **1970**, *3*, 151.
(40) Becke, A. D. *Phys. Rev. A* **1988**, *38*, 3098.
(41) Lee, C. T.; Yang, W. T.; Parr, R. G. *Phys. Rev. B* **1988**, *37*, 785.
(42) Feng, M.; Gao, L.; Du, S. X.; Deng, Z. T.; Cheng, Z. H.; Ji, W.; Zhang, D. Q.; Guo, X. F.; Lin, X.; Chi, L. F.; Zhu, D. B.; Fuchs, H.; Gao, H. J. *Adv. Funct. Mater.* **2007**, *17*, 770.
(43) Frisch, M. J. T., G. W.; Schlegel, H. B.; Scuseria, G. E.; Robb, M. A.; Cheeseman, J. R.; Scalmani, G.; Barone, V.; Mennucci, B.; Petersson, G. A.; Nakatsuji, H.; Caricato, M.; Li, X.; Hratchian, H. P.; Izmaylov, A. F.; Bloino, J.; Zheng, G.; Sonnenberg, J. L.; Hada, M.; Ehara, M.; Toyota, K.; Fukuda, R.; Hasegawa, J.; Ishida, M.; Nakajima, T.; Honda, Y.; Kitao, O.; Nakai, H.; Vreven, T.; Montgomery, Jr., J. A.; Peralta, J. E.; Ogliaro, F.; Bearpark, M.; Heyd, J. J.; Brothers, E.; Kudin, K. N.; Staroverov, V. N.; Kobayashi, R.; Normand, J.; Raghavachari, K.; Rendell, A.; Burant, J. C.; Iyengar, S. S.; Tomasi, J.; Cossi, M.; Rega, N.; Millam, N. J.; Klene, M.; Knox, J. E.; Cross, J. B.; Bakken, V.; Adamo, C.; Jaramillo, J.; Gomperts, R.; Stratmann, R. E.; Yazyev, O.; Austin, A. J.; Cammi, R.; Pomelli, C.; Ochterski, J. W.; Martin, R. L.; Morokuma, K.; Zakrzewski, V. G.; Voth, G. A.; Salvador, P.; Dannenberg, J. J.; Dapprich, S.; Daniels, A. D.; Farkas, Ö.; Foresman, J. B.; Ortiz, J. V.; Cioslowski, J.; Fox, D. J.; *Gaussian*, Revision A.1 ed.; Gaussian, Inc.: Wallingford, CT, 2009.
(44) Prakash, A.; Ouyang, J.; Lin, J. L.; Yang, Y. *J. Appl. Phys.* **2006**, *100*, 054309.
(45) Liu, G.; Ling, Q. D.; Teo, E. Y. H.; Zhu, C. X.; Chan, D. S. H.; Neoh, K. G.; Kang, E. T. *ACS Nano* **2009**, *3*, 1929.
(46) Li, H.; Jin, Z. N.; Li, N. J.; Xu, Q. F.; Gu, H. W.; Lu, J. M.; Xia, X. W.; Wang, L. H. *J. Mater. Chem.* **2011**, *21*, 5860.
(47) Surin, M.; Sonar, P.; Grimsdale, A. C.; Mullen, K.; De Feyter, S.; Habuchi, S.; Sarzi, S.; Braeken, E.; Heyen, A. V.; Van der Auweraer, M.; De Schryver, F. C.; Cavallini, M.; Moulin, J. F.; Biscarini, F.; Femoni, C.; Roberto, L.; Leclere, P. *J. Mater. Chem.* **2007**, *17*, 728.
(48) Mori, T.; Ko, Y. H.; Kim, K.; Inoue, Y. *J. Org. Chem.* **2006**, *71*, 3232.
(49) Wu, H. M.; Song, Y. L.; Du, S. X.; Liu, H. W.; Gao, H. J.; Jiang, L.; Zhu, D. B. *Adv. Mater.* **2003**, *15*, 1925.
(50) Wen, Y. Q.; Wang, J. X.; Hu, J. P.; Jiang, L.; Gao, H. J.; Song, Y. L.; Zhu, D. B. *Adv. Mater.* **2006**, *18*, 1983.
(51) Ling, Q. D.; Song, Y.; Ding, S. J.; Zhu, C. X.; Chan, D. S. H.; Kwong, D. L.; Kang, E. T.; Neoh, K. G. *Adv. Mater.* **2005**, *17*, 455.